Orientational order parameter of the nematic liquid crystalline phase of *F*-actin

Jorge Viamontes,[1,*] Suresh Narayanan,[2] Alec R. Sandy,[2] and Jay X. Tang[1,†]

[1]*Department of Physics, Brown University, Providence, Rhode Island 02912, USA*
[2]*Advanced Photon Source, Argonne National Laboratory, Argonne, Illinois 60439, USA*

We measured the orientational order parameter of *F*-actin traversing the isotropic-nematic phase transition using a combination of techniques, including fluorescence imaging, local birefringence measurements, and small-angle x-ray scattering. The order parameter approaches a saturated value of 0.75 for actin concentrations above the region of the isotropic-nematic phase transition. This result implies a significant extent of misalignment and consequently entanglement among long actin filaments, even in the nematic phase. We determine the specific birefringence of completely aligned *F*-actin to be $\Delta n_0 = 2.3 \times 10^{-5}$ ml/mg. At concentrations slightly below the isotropic-nematic transition, nonzero values of the order parameter are detected for hours following an initial alignment, indicating extremely slow rotational kinetics of *F*-actin in the entangled networks.

PACS number(s): 87.15.−v, 87.16.Ka, 61.30.Vx, 61.30.Gd

I. INTRODUCTION

The abundant and highly conserved cytoskeletal protein actin is responsible for a myriad of cell functions including motility, division, and structural morphology. Globular actin (*G*-actin) polymerizes in a stochastic manner forming long filaments, called *F*-actin, at physiological salt concentrations. Actin is readily labeled with fluorescent probes, which allows for direct recording of single-filament dynamics [1–3]. *F*-actin is a semiflexible polymer with a diameter of 8 nm and persistence length of 15–18 μm [4–6], which is larger than the average filament length (ℓ) found in living cells. *F*-actin solutions undergo an isotropic- (*I*-) to-nematic (*N*) liquid-crystalline phase transition as a function of concentration. The *F*-actin *I-N* phase transition has been shown to occur at an onset concentration inversely proportional to ℓ [7–10], which is consistent with the statistical mechanical theory developed by Onsager, Flory, and many others [11–13]. In a recent publication we have shown that the formation of the *N* phase for *F*-actin with an average filament length $\geqslant 2.7$ μm is continuous in both filament alignment and local concentration [10]. In contrast, for filament lengths $\leqslant 2$ μm the *F*-actin solution undergoes a first-order phase transition [14]. Tactoidal droplets of coexisting isotropic and nematic domains form, showing clearly that it undergoes a discontinuous phase transition. It has been argued that perhaps due to the extreme filament length, polydispersity, and semiflexibility, a combined outcome of defect suppression and entanglement renders the *F*-actin *I-N* transition continuous for long filaments [10]. The continuous *I-N* phase transition may be relevant to the theory of Lammert, Rokshar, and Toner (LRT) [15,16], which predicts that a high disclination line defect energy renders the *I-N* transition into two continuous transitions.

The orientational order parameter (*S*) is a quantitative measure of the level of molecular alignment of the *I-N* phase

transition. Several methods are available to measure *S*, including local birefringence measurements, x-ray scattering, and single-filament imaging. Birefringence microscopy is the most readily available and most convenient to perform. The minimal setup requires only an optical microscope with cross polarizers; thus, the technique has been extensively used for phase transition studies of filamentous suspensions [7–10,14,17]. Small-angle x-ray diffraction has been a standard technique for measurement of *S* and been applied to the liquid-crystal solutions of a number of biological polymers [17–19]. Single-filament imaging provides direct visualization of the orientation of a large number of individual filaments from which *S* can be calculated. Implementation of this technique requires a fluorescence microscope and a high-sensitivity camera. The procedure to obtain the order parameter is straightforward, although it can be a laborious task to acquire sufficiently large number of images required. As a recent example, Dogic *et al.* extracted *S* of the nematic suspension of fd viruses by imaging fluorescently labeled *F*-actin doped in as tracer filaments [3].

We report the orientational order parameter of the liquid-crystalline phase of *F*-actin, measured for selected filament lengths. This work integrates the three techniques and determines reliably the order parameter of *F*-actin in the nematic phase. When performed alone, each technique has its limitations. For small-angle x-ray scattering, it is difficult to fully align the nematic director of *F*-actin along the x-ray capillary tube [19]. Using the fluorescence imaging technique, visualization of single *F*-actin in concentrated samples has a limited time interval of discernable contrast on the order of hours. We have performed measurements using both methods despite their respective limitations. In addition, since *S* and the specific birefringence are proportional [20], *S* can be conveniently obtained using the far simpler birefringence technique, provided that a proportionality constant between the order parameter and the specific birefringence of *F*-actin is determined at a selected sample condition. We explain in this work that such a proportionality constant can be expressed in the form of the saturated specific birefringence, which corresponds to complete filament alignment. We

---

*Present address: Shell International EP, Inc., 3737 Bellaire Blvd., Houston, TX 77025 USA.

†Corresponding author. Electronic address: Jay_Tang@Brown.edu

determine this constant to have a value of $\Delta n_{sat} = 2.3 \times 10^{-5}$ ml/mg for F-actin.

II. MATERIALS AND METHODS

A. Sample preparation

Actin is extracted from rabbit skeletal muscle by the method of Pardee and Spudich [21]. The globular form of the protein, G-actin, is purified using the pharmacia fast protein liquid chromatography (FPLC) system. The purified G-actin is rapidly frozen in aliquots using liquid nitrogen and stored at $-80\,°C$. On the day of experiments the frozen actin is quickly thawed to $25\,°C$, by placing the test tube inside a heatblock, followed by a quick 5 min centrifugation at 7200 g to remove trace amounts of denatured protein. G-actin is polymerized upon the addition of KCl and MgCl$_2$ to the concentration of 50 mM and 2 mM, respectively. Dilution of a G-actin stock solution of 8.3 mg/ml to desired concentrations is performed before actin polymerization. This sequence in the sample preparation is necessary to ensure uniformity in protein concentration and avoid increased pipetting errors due to the increase in viscosity, which accompanies the polymerization of the actin solution. The average filament length of F-actin varies from preparation to preparation depending on how rigorously the minute amount of impurity is removed by discarding fractions of the output from of the FPLC column. It is known that a key regulator of filament length of F-actin is the capping protein, Cap-Z [22], which blocks the fast growing end of F-actin. Assuming that each reconstituted filament is capped by a single capping protein at its plus end, a preparation yielding an average filament length $l=10$ μm indicates that there is 1 capping protein per 3700 actin molecules in molar ratio. This minute amount of impurity is beyond the resolution of typical biochemical assays. In practice, we try to determine l for each preparation, and the values found from our repeated preparations are typically between 5 μm and 12 μm. All experiments in this paper were performed using a preparation of actin that yielded $l=5.6$ μm. To further reduce the filament length we added the actin severing and end capping protein gelsolin [23,24]. Various molar ratios of gelsolin to actin are used in our experiments, as indicated on the relevant figures in the results section. However, the average filament length was not determined for these various samples due to the laborious nature of the procedure. Such an effort was taken in a separate study, for which length plays a more crucial role [14].

A microchannel cell with cross-sectional dimensions of 30×76 μm^2 is used to align F-actin under shear forces (Fig. 1). The channels are constructed by acid etching a standard 2.5-cm-wide microscope glass slide, followed by bonding another microscope slide onto the etched slide. The microchannels are very robust, due to the thick (~ 1.2 mm) slides used for the channel walls, which can endure a pressure of 200 psi. The microscope slides have negligible strain birefringence, and thus such a microchannel assembly is suitable for birefringence measurements. Single-filament fluorescence imaging, however, cannot be performed using this assembly, since the thickness of the slide is beyond the work-
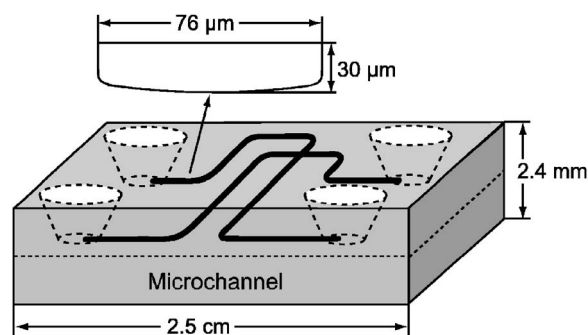

FIG. 1. Skematic of a microchannel cell with channels of cross-sectional dimensions of 30×76 μm^2. A cross-sectional view of the channels is shown above. A slight curvature across the channel on the bottom surface is the result of the acid etching technique.

ing distance of the high-magnification objectives. A pump pressure of 66 psi is used to initiate flow of the F-actin solution into the microchannel. All measurements are followed with a cleaning procedure consisting of flowing ~ 2 ml of water through the used microchannel at a pressure of 200 psi. The retardance measurements of the cleaned microchannel yield negligible values of $0.1-0.2$ nm, which are indistinguishable from that of a new sample. Therefore, the cleaning procedure proves to be effective.

Rectangular capillary tubes from VitroCom Inc. (Mt. Lakes, NJ) of cross-sectional dimensions of 0.05×0.5 mm^2 and wall thickness of 125 μm are used to image the F-actin alignment through fluorescence microscopy and birefringence measurements. Injection into the capillary tube is performed gently (~ 50 μl/min) to avoid filament breakage. Flow is terminated by sealing both ends of the capillary tube with an inert glue. The capillary tubes are prepared for a single use only, since due to their fragile geometry, it proves impractical and ineffective to clean them afterwards.

B. Birefringence and fluorescence measurements

Birefringence measurements are performed on a Nikon TE800 microscope equipped with the commercial CRI PolScope package (Cambridge Research, Inc., Worcester, MA). The PolScope is capable of measuring the optical birefringence and the orientation of the slow axis at each pixel position, thus reporting both local values of birefringence and alignment [25,26]. F-actin is gently injected into a microchannel with cross-sectional dimensions of 30×76 μm^2. The PolScope is used to measure optical retardance as a function of actin concentration and of gelsolin to actin ratio (G/A) (a higher ratio corresponds to a shorter average filament length).

Fluorescence measurements are performed with the same microscope and Photometrics Cool-Snap HQ high-resolution camera bundled with the MetaMorph software (Universal Imaging Inc., Chicago, IL). F-actin is labeled with tetramethylrhodamine isothiocyanate (TRITC) conjugated phalloidin (Sigma, St. Louis, MO) and introduced at a tiny concentration of 8×10^{-4} mg/ml into the concentrated sample. Phalloidin-stabilized F-actin is structurally similar to unlabeled F-actin [4,27]. Labeled F-actin is mixed with the un-

labeled actin, allowing single filaments to be visible while they interact with an ocean of nonlabeled filaments. Labeled filaments are imaged at the center of the capillary tube—i.e., ~25 μm from the top or bottom wall and a distance greater than 100 μm from the side walls. The time interval within which the contrast of the labeled filaments with the background remains suitable for computerized image analysis is approximately 2 h. Such a rapid depreciation of image quality is due to the stochastic exchange of TRITC-phalloidin for nonlabeled phalloidin. All measurements of single F-actin are performed after an initial wait at 25 °C for 1 h from the point in time when the capillary flow became visually undetectable. To reduce photobleaching, an antibleaching buffer was used, containing 16 μg/ml catalase, 0.4 mg/ml glucose, 80 μg/ml glucose oxidase, and 0.2 vol. % mercaptoethanol [1].

C. Single-filament tracing

A large number of fluorescently labeled actin filaments are imaged as a direct method to determine the orientational order parameter of selected samples. Still images of 0.2-s exposures are taken at different positions along the length of the capillary tube. A set of 600 images is collected for each actin concentration. Only labeled filaments whose entire contour length lies within the depth of focus are selected. This selection process, with a typical efficiency of ⩽3 filaments per image, is the only aspect in the analysis where human discretion is involved. F-actin has a diameter of 8 nm, as determined by x-ray crystallography [6,28]. When imaged under a fluorescence microscope, however, the filaments appear to be ≈0.5 μm in diameter due to optical diffraction. To find the center of the filament, image analysis is necessary, the details of which are described below.

Image analysis is performed in MatLab 7.0 (The Math-Works, Inc., MA). The image is threshold processed for bright objects, and a series of morphological operations renders a one-pixel-thick line along the filament, which is defined as the intensity thread [Fig. 2(a)]. The intensity thread is almost always along what appears to be the center of the filament. A line scan is made at every 18° in orientation at every point along the intensity thread. The intensity profiles are expected to be Gaussian in shape. A fitting routine finds the line scan with the least spread, which naturally is the line scan perpendicular to the local contour direction of the filament. The position of the maximum of a parabola best fit to the line scan with the least spread is defined as the center of the filament. Although the routine only uses the line scan with the least spread, we find that the center is unchanged for a series of line scans at oblique angles to the filament [Fig. 2(b)]. Such a process is repeated at every pixel along the intensity thread to determine a collection of points that lie along the center of the filament. This collection of points defines a thin line, which we refer as the filament thread [Fig. 2(c)]. Finally, the filament thread is divided into segments, the orientation of which is analyzed to calculate the orientational order parameter using Eq. (3). In a similar treatment, Dogic *et al.* [3] restricted the segment lengths to ⩾0.5 μm. Below this they noted an unreliable fitting of the tangent-
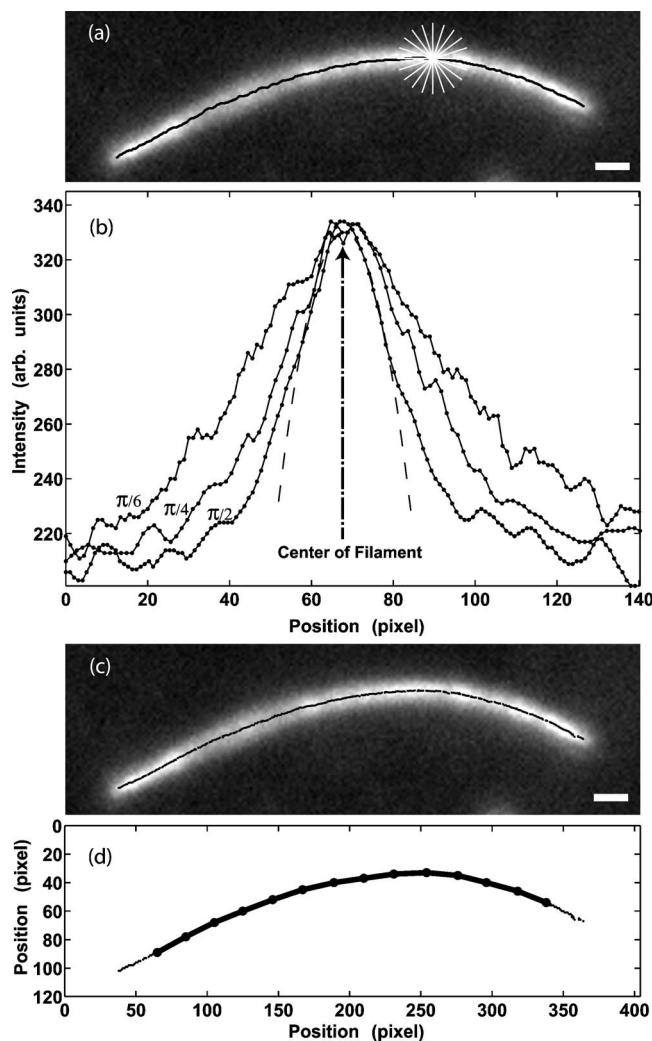

FIG. 2. Fluorescence imaging and analysis of F-actin: (a) An intensity thread (black line) is used as a guide to a series of line scans, depicted as a rosette of white lines. (b) The line scans are Gaussian in shape with the minimal spread for the line scan perpendicular to the local axis of the filament. The line scans of three orientations are shown, with the angles from the x axis indicated. The center of the filament is the maximum of the best fit parabola (dashed lines) as pointed out by the dashed arrow. (c) The center of filament (black line) is shown as calculated from line scans perpendicular to the local direction of the filament. This line is called the filament thread. (d) Segmentation of the filament thread into ~1 -μm sections in size (black line terminated in circles). The scale bars in (a) and (c) represent 1 μm in length.

tangent correlation function for wormlike micelles in a nematic fd background to the theoretically predicted function [29]. A combination of compromising factors may account for the unreliability, including microscope resolution, camera noise, pixelation, and extrapolation errors. We have accordingly chosen the segmentation length to be 1 μm for all the filaments in our study, thereby safely avoiding the unreliability. Filament ends are always investigating the surrounding network by rapid fingering and reptative motion. We choose, therefore, to neglect the end segments such that the contour distance from the tips of the filament thread to the end of the

closest segment is $\geqslant 1$ μm, as shown in Fig. 2(d).

D. Calculation of the order parameter

The orientational order parameter is defined as

$$S = \int P_2(\theta)f(\theta)d\Omega, \tag{1}$$

where $P_2(\theta)$ is the second Legendre polynomial and $f(\theta)d\Omega$ is the probability of a filament to have its long axis within a solid angle $d\Omega$ around an angle θ with respect to the z axis. $f(\theta)$ is called the orientational distribution function (ODF). The z axis is set parallel to the nematic director. S takes the value of 1 for a perfectly aligned system and 0 for an isotropic distribution.

When the filaments in solution are not straight rods, but rather semiflexible polymers, it is necessary to subdivide long filaments into short and relatively straight segments in order to calculate S, as described by Dogic and colleagues [3]. We thus apply the modified expression below to calculate the order parameter:

$$S = \frac{1}{L}\int_0^L dz \int P_2(\theta)F(z,\theta)d\Omega, \tag{2}$$

where L is the filament length and $F(\theta)d\Omega$ is similar to $f(\theta)d\Omega$, but now applies to the distribution of segments, instead of the entire filaments, since in uniaxial nematics F is locally a function of only θ; i.e., the ϕ term is absent [30]. For a large number of segments with a finite length, Eq. (2) can be written as

$$S = \frac{\sum_{j=1}^{N}\sum_{i=1}^{n}\left[\frac{3}{2}\cos^2(\theta_{ij}) - \frac{1}{2}\right]\sin(\theta_{ij})}{\sum_{j=1}^{N}\sum_{i=1}^{n}\sin(\theta_{ij})}. \tag{3}$$

The θ values are for each of the ith segments in the jth filament. The number of filaments at a certain filament length bin size is N, each having n number of segments. The order parameter can be calculated from the distribution of the orientation of each segment of the filaments using Eq. (3). Equivalently, the form of Eq. (2) can be used provided an ODF. The functional form of the ODF is not exactly known, and a series of trial functions is available such as the ones used by Onsager [11,30], Odijk [13], and Oldenbourg *et al.* [18]. Calculations of S obtained through Eq. (2) with the Odijk ODF yield identical results to those of Eq. (3) for $N > 50$, within the fitting errors of our MATLAB routines.

E. Small angle x-ray scattering

Small-angle x-ray scattering (SAXS) measurements were performed at 8-ID-I beamline at the Advanced Photon Source. A monochromatic beam with an energy of 7.5 keV was used, and the incident photon flux was 1×10^{10} photons/s over a beam area of 0.05×0.05 mm^2. A direct-illuminated charge-coupled-device (CCD) detector (Princeton Instruments EEV 1300×1340) was used to collect the scattering pattern. F-actin was injected into a 0.7

-mm quartz x-ray capillary (Charles Supper Company, Natick, MA) and sealed with an inert plastic glue at both ends. As the sample was filled, the N director was aligned along the capillary tube but not completely. Consequently a spread of the scattering lobes was observed, and the measured S was reduced. The x-ray beam was intense enough to locally damage the F-actin sample within 10 s of exposure. This damage could be seen as holes lacking birefringence in the N phase under polarization microscopy. To avoid filament damage due to radiation, the flux density on the sample was reduced by increasing the beam size to 0.25×0.25 mm^2 and adding absorbers in the beam, thereby maintaining a total incident photon flux of 1×10^{10} photons/s. To further limit radiation damage, a single spot on the sample was illuminated for less than 10 s and scattering images from several such spots were integrated to improve the signal-to-noise ratio. Analysis of the x-ray diffraction images was performed using MATLAB 7.0 in much the same method as described by Purdy and co-workers [17] to calculate S for the interparticle scattering of fd virus and what Oldenbourg and co-workers [18] employed for tobacco mosaic virus.

The scattering intensity from a continuous distribution of rods $G(\Psi)$ is a one-dimensional integral along ω, which is the angle the filament makes with the x-ray beam:

$$G(\Psi) = \int_0^{2\pi} I_s(\omega)f(\theta)\sin(\omega)d\omega, \tag{4}$$

where $I_s(\omega) = 1/\sin(\omega)$ is the single-filament scattering intensity, $f(\theta)$ is defined as in Eq. (1), and Ψ is the angle measured from the symmetry axis of the scattering lobe. The angles θ, Ψ, and ω are related by $\cos(\theta) = \cos(\Psi)\sin(\omega)$. Angular ($\Psi$) line scans at a constant q are extracted from the scattering intensity plots with a 21×21 pixel averaging area, providing a q resolution of ± 0.0004 Å^{-1}. A Ψ angular line scan is $G(\Psi)$, fitted using a least-squares routine to obtain $f(\theta)$. The overview of such a procedure is shown in Fig. 3. Once the ODF is obtained, we apply Eq. (1) to calculate S. The calculated value of S is expected to be independent of the q value, which was confirmed in the q range of $0.01 \leqslant q \leqslant 0.027$ Å^{-1}.

III. RESULTS

A. Concentration range of the *F*-actin isotropic-to-nematic phase transition

Figure 4 shows the regions of *I-N* transition at several average filament lengths. At low actin concentrations the F-actin solution is in the I phase, corresponding to no orientational order and consequently no birefringence. Within a defined concentration range for each average filament length, the birefringence increases linearly with concentration. At higher concentrations, a plateau of the specific retardance is observed, corresponding to the nematic phase. For example, in F-actin solutions with no gelsolin added partial alignment is noticeable at concentrations above 1.5 mg/ml and the N phase is reached at $\sim$3 mg/ml. As the G/A ratio increases the onset of the *I-N* phase transition shifts to higher actin concentrations. Although the ratios of gelsolin to actin were
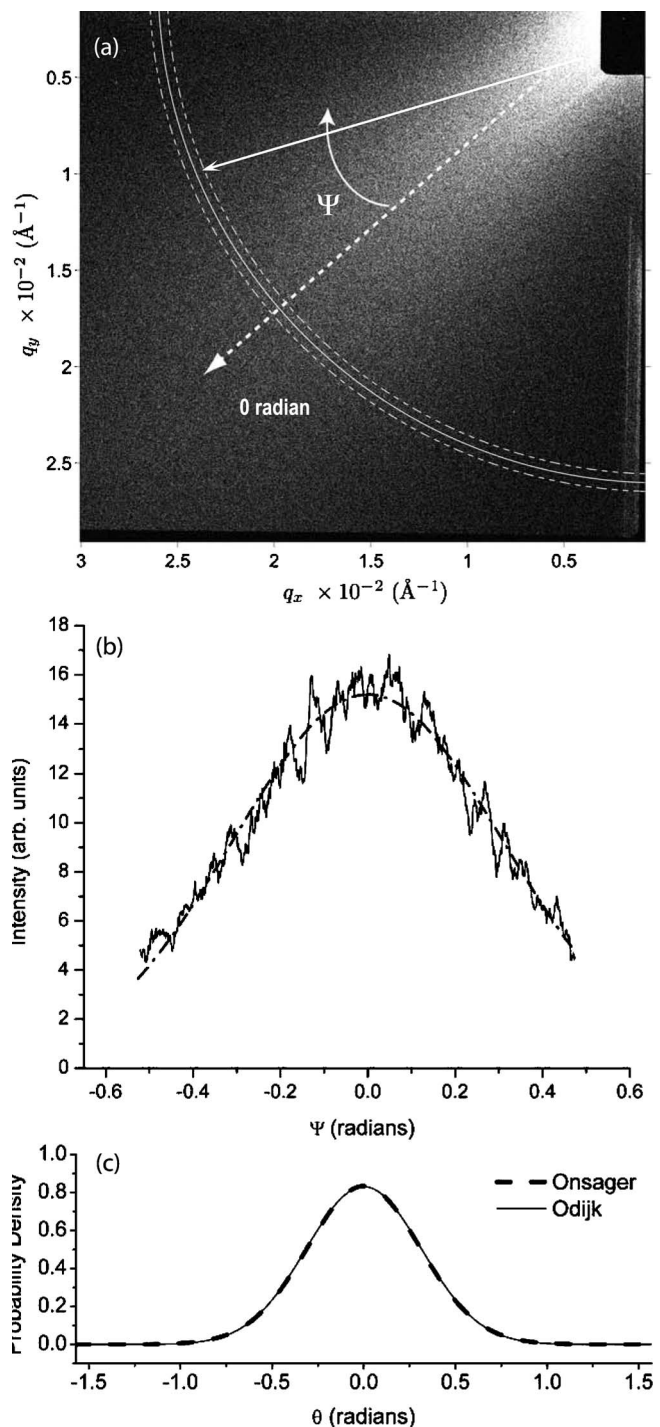
FIG. 3. Small-angle x-ray scattering from F-actin: (a) q_x and q_y intensity scatter plot. A one quadrant image of anisotropic scattering pattern from a suspension of F-actin in the N phase. The 0-rad axis is perpendicular to the capillary axis. The ODF is determined from angular line scans. For example, a thin slice in the range of q = 0.026 ± 0.0004 Å^{-1} is shown enclosed by the white dashed arc lines. (b) The line scan is fitted with Eq. (4), which yields the dash-dotted curve. (c) The normalized Odijk [13] (solid line) and Onsager [11] (dash line) ODF extracted from the data in (b). The curves are indistinguishable.
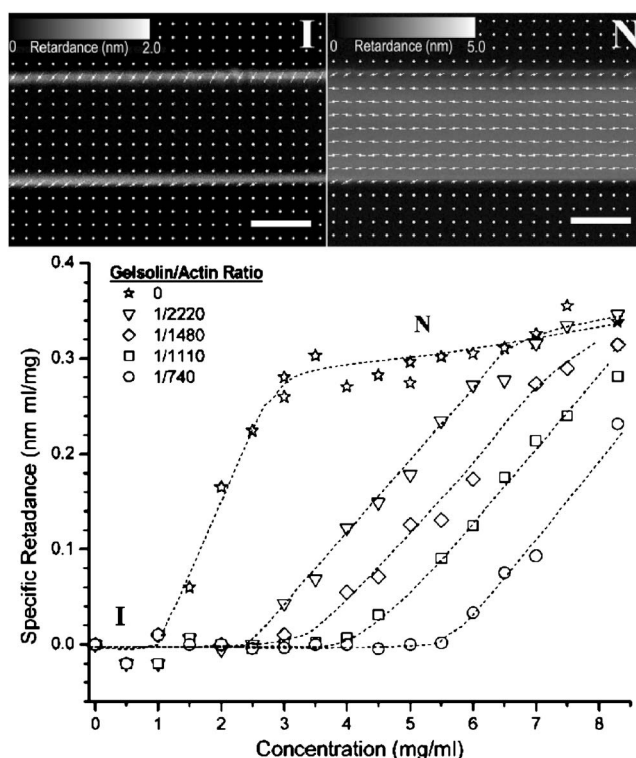

FIG. 4. Specific retardance of F-actin aligned by flow through a 30-μm-thick channel as a function of concentration and filament length indicated by the gelsolin-to-actin ratio. Illustrative examples of the I and N phases are shown at the top row for 0.2 mg/ml and 8 mg/ml, respectively. The image intensity is scaled to represent retardance in nm with slow axis alignment and magnitude depicted by the direction and length of the white segments, respectively. The scale bar represents 40 μm. The onset concentration of the I-N phase transition region increases as the average filament length decreases.

designed to yield an average filament length of 6, 4, 3, and 2 μm, respectively, the actual lengths were shorter than designed and the exact values were not determined (as explained in the sample preparation section). Therefore, we could not obtain a quantitative relation between transition concentration and average filament length from Fig. 4. Nevertheless, we note one reliable feature: that in the nematic phase, all samples tend to reach the same level of alignment, an observation confirmed by other sets of measurements (data not shown).

The I-N phase transition region, characterized by the sharp increase of specific retardance, has been the source of recent studies aimed at determining the order of the phase transition [10,14]. Although Fig. 4 gives a good overview of the phase diagram, the order of the transition cannot be determined from the birefringence measurements alone. Detailed local concentration and filament alignment measurements at the phase transition region were performed, with original findings presented elsewhere [10,14]. Briefly, the I-N phase transition is observed to be continuous for $\ell \geq 2$ μm and discontinuous for $\ell < 2$ μm in both filament alignment and concentration [14]. The "no-gelsolin" condition corresponds to the samples of F-actin of the longest
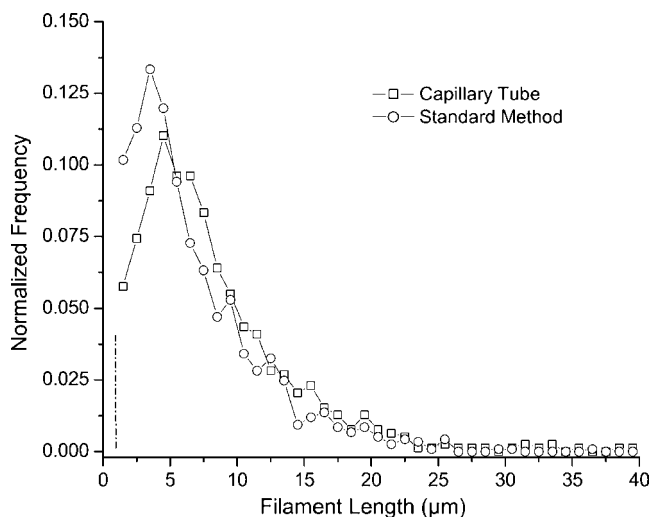
FIG. 5. Filament length distribution of 0.5 mg/ml *F*-actin determined by imaging fluorescently labeled filaments: (□) inside a 0.05x0.5 mm^2 capillary tube, (○) inside a standard coverslip-sample-slide assembly. The dashed line at 1 μm denotes the shortest filament length that can be reliably determined by fluorescence microscopy.

average filament length, the exact value of which depends on the purity of actin. This condition has been the standard for most studies concerning the *I-N* transition of *F*-actin, although not all published studies have determined the average length of *F*-actin in their particular preparations. Nevertheless, in the high actin concentration when the sample is nematic, the alignment is expected to be optimal. Our results also show that the nematic *F*-actin of various average filament lengths have the same extent of alignment, which lead to a common value of order parameter. Thus, in this study, we choose to determine such a common *S* by fluorescence microscopy and x-ray scattering, as presented below.

B. Characterization of filament length distribution

Due to the stochastic process of actin polymerization, *F*-actin is extremely polydisperse. This property plays a key role in a range of physical properties such as filament dynamics and rheology and perhaps also in the range of the phase transition. An important feature of a polydisperse system is the expected partitioning of the filaments with the longer ones concentrating in the nematic phase [31,32]. Through Monte Carlo simulation techniques, Escobedo showed such a partitioning effect in a bidisperse polymer system [31]. Dogic and co-workers [3] showed experimentally a higher-order parameter as the contour length of the probe filaments increased. Therefore, we consider characterizing the length distribution of actin filaments a relevant task in order to define their alignment in the nematic phase.

Filament threads are collected for 700–1200 filaments at each actin concentration for samples filled in capillaries. The contour length distributions typically follow a bell shape (Fig. 5). The average length ℓ and length distribution obtained by manually tracing 1169 filaments prepared by the standard coverslip-sample-slide sandwich are similar to

those obtained with the capillary injection method. Among the two representative sets of data for comparison (Fig. 5), the measured average filament length is 8.1 μm over 780 filaments imaged in the capillery tubes and 6.8 μm over 1169 filaments imaged on the slides, labeled as the standard method. The similar filament length distribution shows that the injection process is strong enough to align the *N* director but gentle enough to keep shear forces from breaking a significant number of filaments. Imaging the filaments inside the capillary is therefore comparable to observing them on a microscope slide. In addition, we note that the filament length distributions at all concentrations of actin above 1 mg/ml are similar not only in shape, but also in the average length ℓ (data not shown).

Although a detailed account of the *F*-actin filament length distribution is beyond the scope of this paper, we would like to mention that such a system has been treated theoretically by many studies [33–35]. Most of these treatments predict an exponential filament length distribution with, to our knowledge, the exception of [35]. The latest work by Bolterauer and co-workers [35] on tubulin assembly retains the exponential decay function for the stochastic nucleation and growth model only. If a catastrophe and rescue mechanism is included, a bell shape distribution similar to that of Fig. 5 emerges when the probability of rescue is not constant throughout the filament. A scenario providing a constant probability of rescue at the position of each monomer along the filament returns the exponential decay result. The applicability of the theory of Bolterauer *et al.* to *F*-actin is still up for debate. Although *F*-actin polymerization and depolymerization dynamics are not as dramatic as those of microtubules, actin filaments may undergo a similar dynamic instability behavior [36], which could account for the observed bell shape distribution. Among the recent studies, the *F*-actin length distribution has been shown to have the predicted exponential decay by some [37–39], but bell shape distributions have been reported by others [1,38]. We have performed measurements of filament lengths by counting up to 6305 filaments in a typical preparation condition without adding gelsolin and confirmed a bell shape distribution. Further theoretical work withstanding, it is important to recognize the polydisperse and nonexponential filament length distribution of *F*-actin, which may be a property of concern to the orientational ordering and certain features of the *I-N* transition of *F*-actin.

C. Measurement of nematic order parameter by fluorescence imaging

Observations of a large number of segmented filament threads in the *I* phase indicate no alignment, as shown in Figs. 6(a) and 6(b). Even long filaments of 9 μm-sized segments are found with completely random orientations, just as their shorter counterparts. In contrast, *F*-actin in the *N* phase is aligned [Figs. 6(c) and 6(d)]. The filaments are found to align along the capillary axis, but with a spread that yields an orientational order parameter less than unity. Figure 6(d) also shows a rare occurrence of one filament severely bent to form a hairpin turn. Hairpin defects such as this, when ob-
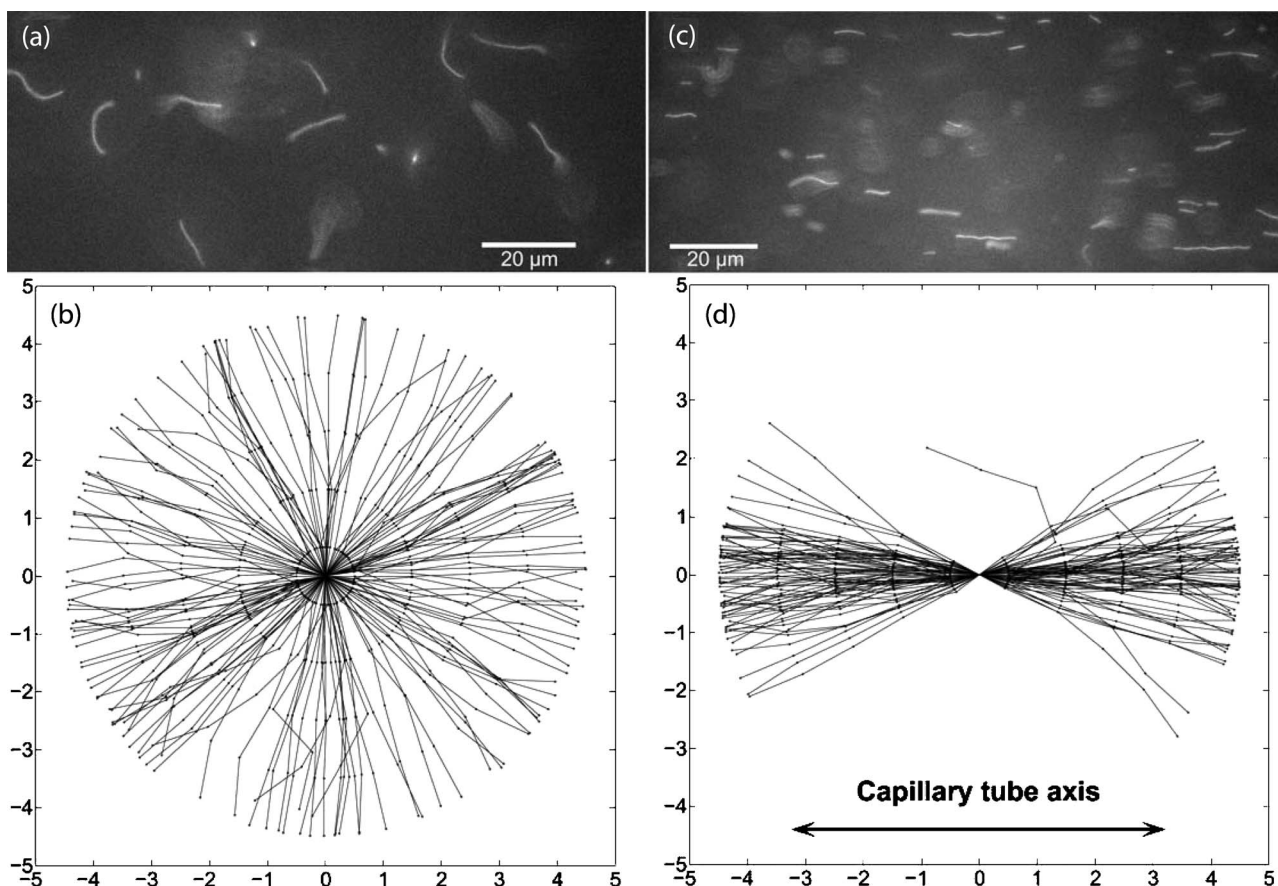
FIG. 6. Filaments nine segments long in the isotropic and nematic liquid-crystalline phases: (a) Individual filament alignment at the I phase with neither axial nor positional order. The actin concentration is 0.2 mg/ml. (b) A collection of 64 filaments of nine segments long is found in the isotropic phase, as the rosette of aligned filaments show. (c) Long-range axial alignment with no positional order is observed for F-actin at the N phase for an actin concentration of 8.0 mg/ml. (d) Seventy-four filaments of nine segments long are found in the nematic phase. All filaments are positioned with the center of filaments at the origin of coordinates. The axial unit length is equal to 1 μm.

served over time, tend to straighten following repeated reptative motions. Similar behavior was observed by Dogic *et al.* [3], in which case F-actin hairpin defects were seen to "pop" out in a background of fd viruses in the N phase. Filaments in Figs. 6(b) and 6(d) are representative subsets of the total filaments acquired at the two actin concentrations. For example, for a 8-mg/ml sample the total number of filaments imaged is 926, out of which 74 filaments possess a length of 9 segments. The number of filaments at each selected length depends on the filament length distribution (Fig. 5). Since the tail end on the filament length distribution is exponential [39], filaments of lengths >15 μm are extremely rare.

Optical birefringence measurements of the same capillary tubes used to gather the fluorescence images are performed after an overnight repose at 4 °C, followed by room-temperature equilibration for 1 h. Optical retardance and filament axis alignment measurements confirm that for G-actin concentrations in the I phase there is no net axial alignment. Similarly, in the I-N phase transition region and for the N phase, filament alignment is predominantly parallel to the capillary axis. Specific retardance measurements correlate well to the data acquired for 30-μm-thick microchannels shown in Fig. 4. In the isotropic phase zero birefringence is seen at low G-actin concentrations followed by the

I-N phase transition region characterized by a linearly increasing specific retardance, which ultimately reaches a plateau beyond the concentration at which the sample becomes completely nematic (Fig. 7).

We proceed to determine S by binning the filaments considered to have short (1–5 segments), medium (6–12 segments), and long ($\geqslant$13 segments) contour lengths to ensure good statistics while comparing the extent of order for various filament lengths. At any actin concentration, the short filaments will be able to rotate, thereby exploring possible reptation tubes more easily than long filaments. Accordingly, a lower S is predicted for short filaments [31,32]. Figure 7 shows such a trend. In the I phase at an actin concentration of 0.2 mg/ml, S is negligible. When the actin concentration is raised while still below the onset concentration of the I-N transition, the entangled isotropic phase is reached. Under entanglement a filament's rotational mobility is drastically reduced, increasing the time required to reach the equilibrium distribution of their orientations. Such slow rotational kinetics can be seen for actin concentrations of 0.5–1 mg/ml. A nonzero S in the entangled I phase indicates that the initial unintended alignment due to the injection of the F-actin solution into the capillary tube is still present 1 h later. Extremely long filaments are affected more by the ro-
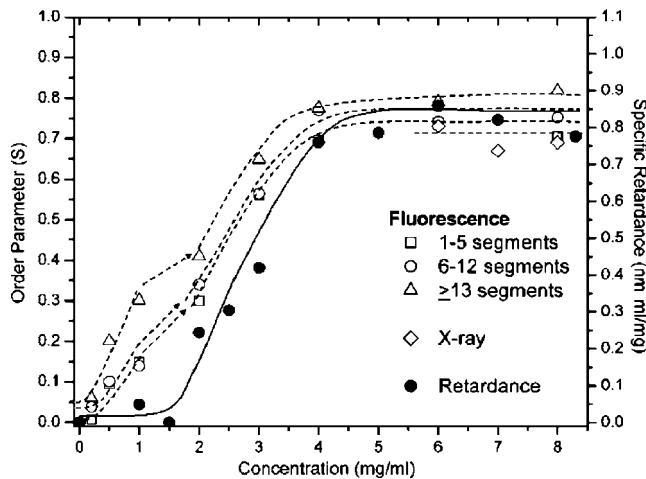
FIG. 7. Order parameter of *F*-actin aligned by flow through a 50-μm-deep channel as a function of actin concentration and filament length binned as indicated in the figure legend for 1–5 segments, 6–12 segments, and 13 segments and above as squares, circles, and triangles, respectively. The order parameter of *F*-actin aligned by flow in a 0.7-mm-diameter x-ray capillary is shown for comparison (diamonds). Specific retardance (solid circles) tracks the order parameter plots. All lines serve as guides for the eye.

tational hindrance and show a greater degree of residual alignment than short- and medium-length filaments. Once a nematic director is established, filaments are drawn to align along the capillary axis. Energetic discouragement for a filament perpendicular to the nematic director favors their alignment towards the selected orientation, and thus slow kinetics does not occur in this region. At the onset of the *I-N* phase transition, a nematic director is established and a nonzero *S* is observed. *S* resumes a linear dependence on concentration in the phase transition region above 2 mg/ml. At high actin concentrations, the *F*-actin solution settles into the *N* phase, indicated by the apparent saturation of the order parameter.

D. Order parameter measured by x-ray scattering

A plateau of *S* is observed once the *N* phase is reached, which correlates well with the plateau for the specific retardance. The *N* plateau value of *S*=0.75 by single-filament imaging and *S*=0.70 by x-ray scattering agree reasonably well. For x-ray scattering experiments, the alignment of the *N* director field along the capillary axis is rather crude, which is expected to lead to a reduced *S*. Recently, Helfer and co-workers measured *S* by x-ray scattering, obtaining values between 0.4 and 0.7 [19]. Such a variability is likely due to the difficulty in aligning the nematic director of *F*-actin samples along the x-ray capillary. Nonetheless, the high end value of Heifer *et al.* of 0.7 is in good agreement with our measurements by both x-ray and fluorescence methods.

E. Specific birefringence of nematic *F*-actin

Theoretically, we expect the sample birefringence Δn to be proportional to *S* and the birefringence of a perfectly aligned *F*-actin solution, Δn_0, as [20,40]

$$\frac{\Delta n_{sat}}{c} = S \frac{\Delta n_0}{c}. \tag{5}$$

For samples with a thickness of 50 μm, the saturated specific retardance is 0.85 nm$\times$ml/mg. Thus the specific birefringence is $\Delta n_{sat}=1.7\times10^{-5}$ ml/mg. A value for *S*=0.75 leads to a $\Delta n_0=2.3\times10^{-5}$ ml/mg for *F*-actin. This result is in good agreement with Helfer *et al.* [19]. This result for *F*-actin is also similar to that of tobacco mosaic virus obtained by Fraden and co-workers [41] and that of microtubules by Bras *et al.* [42], likely due to the common proteinaceous nature among these systems.

IV. DISCUSSION AND CONCLUSIONS

F-actin solutions undergo an *I-N* liquid-crystalline phase transition with respect to both concentration and ℓ. Theoretically, a discontinuous *I-N* phase transition is predicted. At the onset of the nematic phase *S* is predicted to be $\approx$0.8 by Onsager [11] and $\approx$0.7 by Straley [43]. Our measured values of *S*=0.75 by single-filament microscopy and 0.7 by small-angle x-ray scattering agree favorably with these theoretical predictions.

Recent studies of the *I-N* phase transition of *F*-actin are primarily based on optical polarization techniques [7–10]. Although it is a quantitative molecular alignment measurement tool, determination of *S* from birefringence measurements is difficult in *F*-actin solutions, since Δn_0 requires perfectly aligned *F*-actin. We have determined *S* by single filament fluorescence microscopy image analysis and by x-ray scattering, obtaining the useful proportionality constant of $\Delta n_0/c=2.3\times10^{-5}$ ml/mg, and thus allowing the order parameter to be calculated for future optical birefringence measurements. Furthermore, molecular alignment behavior across the *I-N* phase transition also illustrates filament kinetics. At concentrations <0.2 mg/ml the axial randomization inherent in the *I* phase is achieved within 1 h. In the tightly entangled *I* phase (0.5–1.5 mg/ml) rotational hindrance renders *F*-actin with diminished rotational motion. Consequently, in the time window provided by our experiment we measure a nonzero *S* for the entangled *I* phase, a result of the unintended initial filament alignment caused by injecting the sample. Motions of individual filaments are severely hindered by the constraining tube. Such a constraint is even more severe for longer filaments. Therefore, long filaments show a greater degree of residual alignment after 1 h than short filaments. Due to the stochastic exchange of TRITC-phalloidin for phalloidin and vice versa, image contrast is reduced to the sensitivity limit of our image analysis algorithm approximately 2 h after the initial mixing of the labeled and unlabeled *F*-actin. Therefore, the time window for imaging is not long enough to allow complete rerandomization of the *F*-actin following injection for the entangled *I* phase (Fig. 7). Once a nematic director is established at the onset of the *I-N* phase transition, the range of the filaments' rotation is reduced by the energetic favorability of aligning parallel to the *N* director. As such, close correlation between *S* and the specific retardance at the *I-N* transition and *N* phase is expected and observed, except at the onset of the

weak alignment region due to the slow kinetics.

Filament entanglement has been suggested in the polymer community as immobilizing long filaments in solution, thereby preventing the establishment of thermodynamic equilibrium. Consequently, the polymer solution may be found in a metastable state and the I-N phase transition could become continuous for long enough ℓ. An actin filament of length 7 μm undulates under $k_B T$ with an amplitude of $\sim$1 μm at the lowest harmonic mode, implicating strong entanglement of F-actin solutions. F-actin entanglement brings about a frequency-independent elastic modulus as observed by Gardel $et\ al.$ [44], reinforcing the entanglement assertion with its possible hindrance of thermodynamic equilibrium for long ℓ.

The theoretical treatment of steric jamming at polymer densities where rotational diffusion is hindered was considered by Edwards and Evans [45]. They studied the motions of a rod diffusing along a reptation tube with gates that open and close randomly through thermal fluctuations. The gating is due to the motions of neighboring filaments protruding into the reptation tube and hampering motions past them, a result of the limited freedom to sidestep the protruding obstacle. They showed that the diffusion of a filament along the reptation tube depends critically upon the cooperation of the surrounding filaments. Furthermore, filaments become more immobilized at increased concentration or filament length. Taking into account the jamming effect, it is reasonable to expect the continuous I-N phase transition for long F-actin.

The recent theory by LRT [15,16] predicts that the weakly first-order I-N transition can break into two continuous transitions, I to topologically ordered isotropic (T), followed by a weakly aligned N phase, if the disclination core energy is raised sufficiently high. An alternative explanation is that thermodynamic equilibrium could be hindered by the filament entanglement and the jamming effect explained above. Recent work by Helfer $et\ al.$ show disclination line defects near the meniscus of a 2-mg/ml F-actin solution [19]. Our observations suggest that such defects are extremely rare and could be caused by the poorly defined shear pattern as the

samples are injected into capillaries. Helfer $et\ al.$ also studied the birefringence patterns after sonication and attributed the pattern formation to the mechanical history of the sample rather than thermodynamics. Entanglement could play an important role in explaining the mechanical stress dependence of the pattern [14]. Clearly, further studies are called for to assess the thermodynamic origin of such an interesting ℓ dependence of the I-N phase transition of F-actin.

In summary, by direct imaging of filaments in the nematic phase, we have determined the orientational order parameter to reach a saturating value of 0.75 when filaments of various lengths are averaged. A similar value is obtained by x-ray scattering measurements. A saturated specific birefringence value of nematic F-actin is determined for the same sample. By comparing these values, we determine the specific birefringence of completely aligned F-actin to be $\Delta n_0/c = 2.3 \times 10^{-5}$ ml/mg. This value is useful for determining the order parameter of F-actin at various lengths and solution conditions in the future, solely by birefringence measurements, which can be conveniently performed in small laboratories. The results of this work show clearly a noticeable width of the I-N transition region and slow kinetics coupled with the transition for solutions of long filaments. However, this work does not address the expected first-order nature of the phase transition and the issues such as phase separation and coexistence.

[1] J. Kas, H. Strey, J. Tang, D. Finger, R. Ezzell, E. Sackmann, and P. A. Janmey, Biophys. J. **70**, 609 (1996).

[2] J. Kas, H. Strey, and E. Sackmann, Nature (London) **368**, 226 (1994).

[3] Z. Dogic, J. Zhang, A. W. C. Lau, H. Aranda-Espinoza, P. Dalhaimer, D. E. Discher, P. A. Janmey, R. D. Kamien, T. C. Lubensky, and A. G. Yodh, Phys. Rev. Lett. **92**, 125503 (2004).

[4] H. Isambert, P. Vernier, A. C. Maggs, A. Fattoum, R. Kassab, D. Pantaloni, and M. F. Carlier, J. Biol. Chem. **270**, 11437 (1995).

[5] F. Gittes, B. Mickey, J. Nettleton, and J. Howard, J. Cell Biol. **120**, 923 (1993).

[6] K. C. Holmes, D. Popp, W. Gebhard, and W. Kabsch, Nature (London) **347**, 44 (1990).

[7] C. Coppin and P. Leavis, Biophys. J. **63**, 794 (1992).

[8] R. Furakawa, R. Kundra, and M. Fechheimer, Biochemistry **32**, 12346 (1993).

[9] A. Suzuki, T. Maeda, and T. Ito, Biophys. J. **59**, 25 (1991).

[10] J. Viamontes and J. X. Tang, Phys. Rev. E **67**, 040701(R) (2003).

[11] L. Onsager, Ann. N.Y. Acad. Sci. **51**, 627 (1949).

[12] P. J. Flory, *Statistical Mechanics of Chain Molecules* (Interscience, New York, 1969).

[13] T. Odijk, Macromolecules **19**, 2313 (1986).

[14] J. Viamontes, P. W. Oakes, and J. X. Tang, e-print cond-mat/0506813/physics/0604212.

[15] P. E. Lammert, D. S. Rokhar, and J. Toner, Phys. Rev. Lett. **70**, 1650 (1993).

[16] P. E. Lammert, D. S. Rokhar, and J. Toner, Phys. Rev. E **52**, 1778 (1995).

[17] K. R. Purdy, Z. Dogic, S. Fraden, A. Ruhm, L. Lurio, and S.

G. J. Mochrie, Phys. Rev. E **67**, 031708 (2003).

[18] R. Oldenbourg, X. Wen, R. B. Meyer, and D. L. D. Caspar, Phys. Rev. Lett. **61**, 1851 (1988).

[19] E. Helfer, P. Panine, M. F. Carlier, and P. Davidson, Biophys. J. **89**, 543 (2005).

[20] G. Maret and K. Dransfeld, in *Strong and Ultrastrong Magnetic Fields and Their Applications*, edited by F. Herlach (Springer-Verlag, New York, 1985), p. 151.

[21] J. Pardee and J. Spudich, Methods Cell Biol. **24**, 271 (1982).

[22] J. Casella, E. Barron-Casella, and M. Torres, Cell Motil. Cytoskeleton **30**, 164 (1995).

[23] P. Janmey, J. Peetermans, K. Zaner, T. P. Stossel, and T. Tanaka, J. Biol. Chem. **261**, 8357 (1986).

[24] J. X. Tang and P. A. Janmey, J. Biol. Chem. **271**, 8556 (1996).

[25] R. Oldenbourg and G. Mei, J. Microsc. **180**, 140 (1995).

[26] M. Shribak and R. Oldenbourg, Appl. Opt. **42**, 3009 (2003).

[27] M. O. Steinmetz, D. Stoffler, S. Muller, W. Jahn, B. Wolpensinger, K. Goldie, A. Engel, H. Faulstich, and U. Aebi, J. Mol. Biol. **276**, 1 (1998).

[28] J. Hanson and J. Lowly, J. Mol. Biol. **6**, 46 (1963).

[29] D. Daniels and M. Turner, Macromolecules **38**, 182 (2005).

[30] P. de Gennes and J. Prost, *The Physics of Liquid Crystals*, 2nd ed. (Oxford Science, New York, 1993).

[31] F. A. Escobedo, J. Chem. Phys. **118**, 10262 (2003).

[32] H. Lekkerkerker, P. Coulon, R. van der Haegen, and R. Deblieck, J. Chem. Phys. **80**, 3427 (1984).

[33] F. Oosawa and S. Asakura, *Thermodynamics of the Polymerization of Protein* (Academic Press, New York, 1975), p. 34–35.

[34] J. N. Israelachvili, *Intermolecular and Surface Forces* (Academic Press, New York, 1991), Chap. 16.

[35] H. Bolterauer, H. J. Limbach, and J. Tuszynski, Bioelectrochem. Bioenerg. **48**, 285 (1999).

[36] I. Fujiwara, S. Takahashi, H. Tadakuma, T. Funatsu, and S. Ishiwata, Nat. Cell Biol. **4**, 666 (2002).

[37] T. Oda, K. Makino, I. Yamashita, K. Namba, and Y. Maeda, Biophys. J. **75**, 2672 (1998).

[38] S. Burlacu, P. Janmey, and J. Borejdo, Am. J. Physiol. **262**, C569 (1992).

[39] D. Sept, J. Xu, T. D. Pollard, and J. A. McCammon, Biophys. J. **77**, 2911 (1999).

[40] R. Oldenbourg and T. Ruiz, Biophys. J. **56**, 195 (1989).

[41] S. Fraden, G. Maret, and D. L. D. Caspar, Phys. Rev. E **48**, 2816 (1993).

[42] W. Bras, G. Diakun, J. F. Diaz, M. G. Kramer, J. Bordas, and F. J. Medrano, Biophys. J. **74**, 1509 (1998).

[43] J. P. Straley, Mol. Cryst. Liq. Cryst. **22**, 333 (1973).

[44] M. L. Gardel, M. T. Valentine, J. C. Crocker, A. Bausch, and D. A. Weitz, Phys. Rev. Lett. **91**, 158302 (2003).

[45] S. Edwards and K. Evans, J. Chem. Soc., Faraday Trans. 1 **78**, 113 (1982).